Int. J. Electrochem. Sci., 12 **(2017)** 8806 – 8819, doi: 10.20964/2017.09.17

International Journal of
ELECTROCHEMICAL
SCIENCE
www.electrochemsci.org

The Corrosion Behavior of 316L Stainless Steel in H_2S environment at high temperatures

Lei Zhang[*], *Xian Tang, Zhu Wang, Ting Li, Ziru Zhang, Minxu Lu*

Institute of Advanced Materials and Technology, University of Science and Technology Beijing, Beijing 100083, PR China
[*]E-mail: zhanglei@ustb.edu.cn

Received: 25 May 2017 / *Accepted:* 1 July 2017 / *Published:* 13 August 2017

The corrosion behavior of 316L stainless steel was studied by electrochemical measurements, X-ray photoelectron spectroscopy (XPS) analysis and Auger electron spectroscopy (AES) analysis. Potentiostatic results show that the presence of H_2S can make 316L more sensitive to temperature. The coexistence of H_2S and Cl^- can obviously decrease the corrosion resistance of 316L stainless steel comparing with H_2S-free condition. XPS analysis shows that the passive film formed under H_2S-containing condition is composed of FeS_2, NiO, NiS, Cr_2O_3 and $Fe(OH)_2$. AES analysis shows that elemental S and Cl can penetrate into the passive film and induce deterioration of the passive film.

Keywords: Stainless steel, hydrogen sulfide, temperature, XPS, AES

1. INTRODUCTION

The corrosion problem during oil field exploitation, gathering and transportation greatly affects the production of each operator sustain abilities. Since the corrosion induces potential security risk, it will be possible to bring incalculable economic losses to the owners of oil fields, to damage the environment around the work area, to pose a great threat to the safety of people [1, 2]. Because of their better corrosion resistance than that of carbon steel, stainless steels are widely used in the construction and operation of the oil fields [3, 4]. 316L stainless steel has been widely used in oil and gas fields due to its good corrosion resistance, low cost and suitable mechanical characteristics.

Stainless steels owe their superior corrosion resistance to the passive films on surface [5-8]. Generally, the passive film mainly consists of Fe_2O_3, $Fe(OH)_3$ and Cr_2O_3[9]. The protectiveness of the passive film depends largely on the chromic oxide. In general, Cr can promote the formation of a protective surface oxide and Ni can enhance the stability of the protective oxide, and thus, a higher

amount of Cr and Ni in the composition of the stainless steel can provide a better performance of alloys.[10].

The effect of temperature on the passive behavior of stainless steel has been studied by a lot of researchers. Ashida [11] found that the corrosion potential increase from -293mV to -256mV (Ag/AgCl) when temperature was decreased from 102^{o}C to 72^{o}C, and passive current density increase exponential over the temperature range 65^{o}C to 95^{o}C. Zhang [12] found that increasing temperature leads to thickening of both layers which improves passivity, but also leads to loss of Cr_2O_3 from inner and Mo/Cu from outer layers. Under the condition of coexistence of H_2S and Cl^-, passive film may be more sensitive to temperature, which significantly affects the corrosion rate, corrosion mechanism and the properties of the material surface.

Meanwhile, the passive film adapts to changes in potential or anion concentration in the electrolyte, and the dynamic properties of the passive film provide the key to the high resistance of stainless steel to corrosive attacks [13]. However, the presence of H_2S, CO_2, and Cl^- may still lead to severe corrosion failures of materials, such as pitting and stress corrosion creaking (SCC)[14].The passive behavior of stainless steel in H_2S-Cl^- environments have received a lot of attention in recent years. Banas[15] reported that they found a negative effect of H_2S on oxide stability of austenitic steel, and the film does not constitute a protective film. He[16] found that Cl^- concentration had a significant effect on semiconductor properties of the oxide film, while the gases had little effect under the condition of coexistence of H_2S and Cl^-. They also found that sulphur entered the oxide film through local weakening of the oxide by the Cl^-. Ding[17] found that the presence of H_2S in Cl^- solution can accelerate both the cathodic and anodic current density, changing the semiconductor behavior from p-type to n-type, increasing its susceptibility to corrosion.

This work aims to provide a systematic understanding of the corrosion behavior of 316L in H_2S-Cl^- environment. By combination of potentiodynamic polarization and potentiostatic measurements, the effect of temperature on the corrosion behavior of 316L in the presence and absence of H_2S was evaluated. EIS and cyclic polarization measurements were employed to investigate the synergistic effect of H_2S and Cl^-. Some surface analytical techniques, including the XPS and AES were employed to characterize the chemical composition of the passive film after simulation test.

2. EXPERIMENTAL

2.1 Material and solution

All test specimens were cut from a hot-rolled 316L stainless steel plate. The chemical composition of the stainless steel is shown in Table 1. Samples were cut to the size of 10 mm × 10 mm × 3 mm. Prior to experiment, all specimens were subsequently abraded with decreasing grit size to 2000 SiC paper and cleaned by distilled water and ethanol, then dried by cool air. Solutions contained 5,000 mg/L and 130,000 mg/L Cl^-, were prepared using deionized water and analytically pure NaCl. The solution was deaerated by N_2 for 24 h before use.

Table 1. Chemical composition of 316L austenitic stainless steel (wt%)

Alloy	**C**	**Si**	**Mn**	**P**	**S**	**Cr**	**Mo**	**Ni**	**Fe**
316L	0.022	0.47	1.07	0.024	0.001	18.5	2.13	11.0	Bal.

2.2 Electrochemical measurements

The electrochemical measurements were carried out in a HTHP (high temperature and high pressure) three-electrode autoclave, using a platinum plate as the counter electrode, an Ag/AgCl as the reference electrode and the stainless steel as the working electrode.

The open circuit potential (OCP) measurement was carried out to illustrate the corrosion evolution during the temperature rising process. The OCP was firstly stabilized at the room temperature for 0.5 h, and then the OCP was continuously monitored during the temperature rising process. The temperature was increased at the rate of approximately 80^{o}C/h.

EIS measurements were carried out at OCP using alternating current voltage amplitude of 10 mV. The frequency varied from 100,000 to 0.01 Hz. The potentiodynamic polarization curves were recorded from -0.1 V in positive direction with a potential sweep rate of 0.167 mV/s. The reversing current density was 5 mA/cm^2.

The potentiostatic polarization measurements were conducted at the corresponding potential, which was selected according to the potentiodynamic polarization results. The work electrode was firstly anodically polarized at a constant potential for 0.5 h to stabilize the current density. Afterwards, the temperature was increased at a constant rate to record the *i-t* curve during the temperature rising process.

2.3 XPS analysis

In order to analyze the composition of passive films, XPS experiments were carried out by an AXIS-UltraDLD instrument before and after the immersion tests. A monochromatic Al Kα ($h\upsilon$ = 1486.6 eV) was used as the X-ray source. The C 1s peak at 284.8 eV was used as a reference to correct the charging shifts. Then a commercial software XPSpeak version 4.1 was used to fit the experiment data.

2.4 AES analysis

In order to analysis the element depth profiles of the passive films, AES depth profiles were measured by a PHI -700 scanning Auger Microprobe (ULVAC-PHI, Japan) with a coaxial electron gun and a cylindrical mirror analyzer (CMA) after immersion tests. The Auger spectra were taken at 5 keV with an energy resolution of 0.1%, and the electron incidence angle with respect to the normal average surface plane was 30°. The vacuum level of the analysis chamber during measurement was of

the order of 3.9 × 10^{-9}Torr. The sputtering rate, as determined from thermal oxidation of SiO_2/Si standard, was approximately 17 nm/min vs Si/SiO_2.

3. RESULTS AND DISCUSSION

3.1 Effect of temperature on the corrosion behavior of SS

Fig. 1 presents the OCP variation of 316L in H_2S-free condition vs. temperature and time. From 0 to 0.5 h, i.e. at 25°C, the OCP is much stable, whose value was -0.249 V (vs. Ag/AgCl). With temperature increasing, the OCP showed a decreasing trend, which may be attributed to the acceleration effect of temperature on the anodic reaction. When the temperature reached 120°C, the OCP stabilized at -0.616 V (vs. Ag/AgCl). In general, the OCP decreased for 0.367 V from 25°C to 120°C.

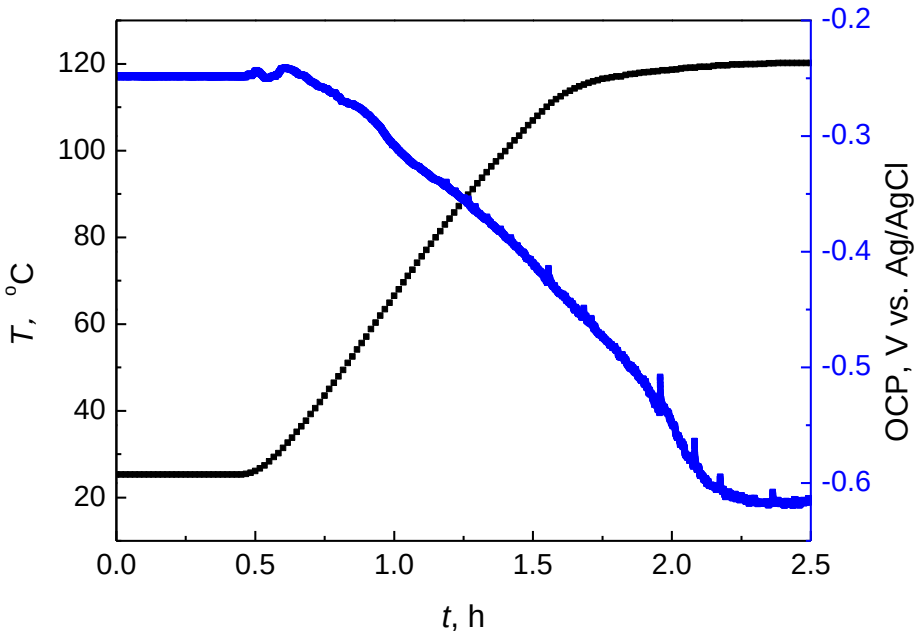

Figure 1. The OCP variation of 316L in H_2S-free condition vs. temperature and time.

The cyclic polarization curves of 316L in H_2S-free condition at different temperatures are shown in Fig. 2. All curves exhibits the current plateau due to the passivation of 316L. The polarization curves moved towards the bottom right and the passive region was much narrowed with temperature increasing, indicating the corrosion resistance decreased. The potential of -0.2 V (vs. Ag/AgCl) was selected from the polarization curves in Fig. 2 as it refers to the potential, which is located in the passive region, regardless of the temperatures. Fig. 3 shows the *i*-*t* and *T*-*t* curves of 316L in H_2S-free condition. As can be seen, the current densities stabilized after polarization for 0.2 h. From 0.5 to 1 h, the current densities slightly increase with temperature (25 to 68°C). After 1.5 h, the current densities drastically increase with temperature (110 to 120°C). With prolonged time, the current densities decreased and finally stabilized at around 50 μA/cm^2. The current peak at 1.9 h

(117°C) may be attributed to the metastable pitting occurred on the sample surface. The above results indicate 316L is temperature sensitive when higher than 110°C, while it is insensitive at temperatures lower than 68°C. This conclusion is in accordance with the polarization results. As shown in Fig. 2, the passive current density increased slightly from 25 to 80°C and then increased for approximately an order of magnitude to 120°C.

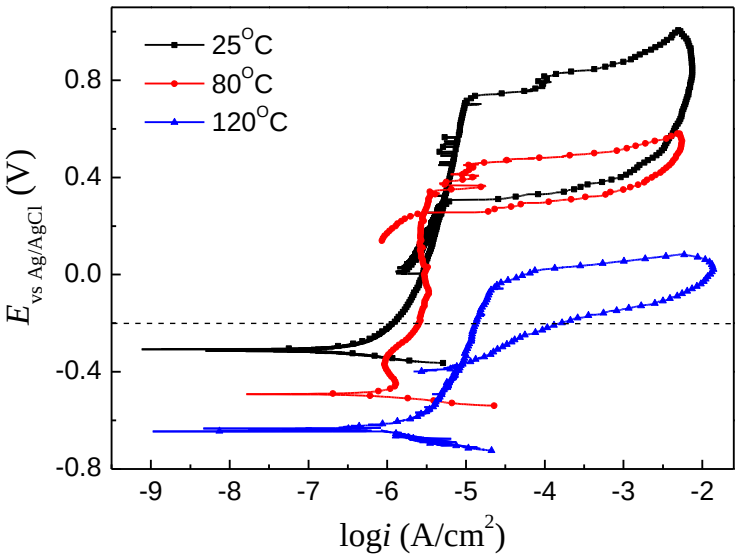

Figure 2. The cyclic polarization curves of 316 L in H_2S-free condition at different temperatures

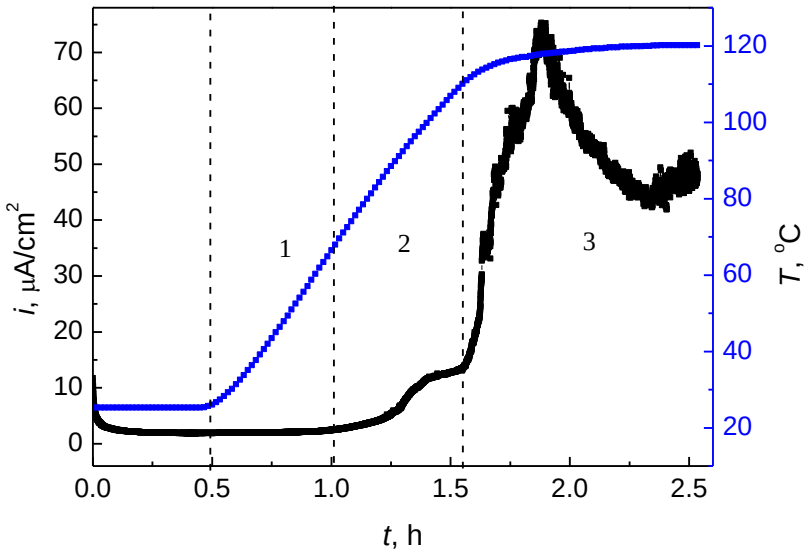

Figure 3. The *i*-*t* and *T*-*t* curves of 316L in H_2S-free condition

The cyclic polarization curves of 316 L in H_2S-containing condition at different temperatures are shown in Fig. 4. Unlike the curves in Fig. 2, the current plateau disappeared at 70 and 120°C. The potentiostatic polarization was also employed at -0.2 V (vs. Ag/AgCl), and the results are shown in Fig. 5. The current densities increased sharply with temperature. At 53°C, the current densities reached 100 μA/cm^2, which is commonly used as the indication for pitting corrosion. In comparison with the

H_2S-free condition, the current densities are much higher, indicating the negative effect of H_2S on the corrosion resistance. Besides, the result also indicates 316L is more sensitive to temperature in H_2S-containing condition.

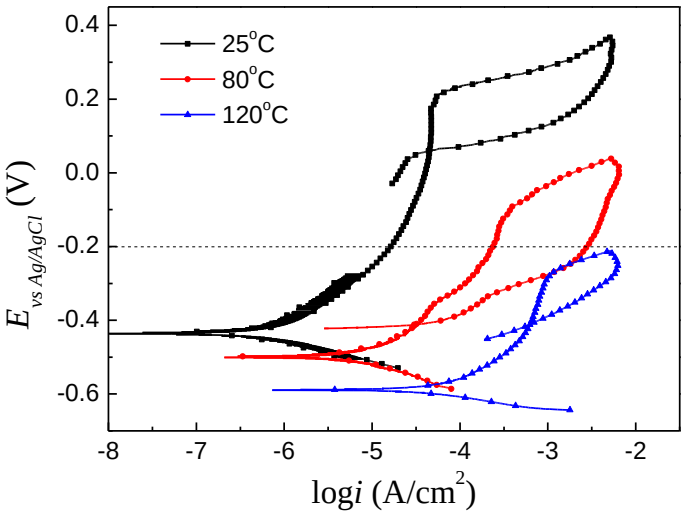

Figure 4. The cyclic polarization curves of 316 L in H_2S-containing condition at different temperatures. The partial pressures of H_2S and CO_2 are 100 kPa and 500 kPa, respectively.

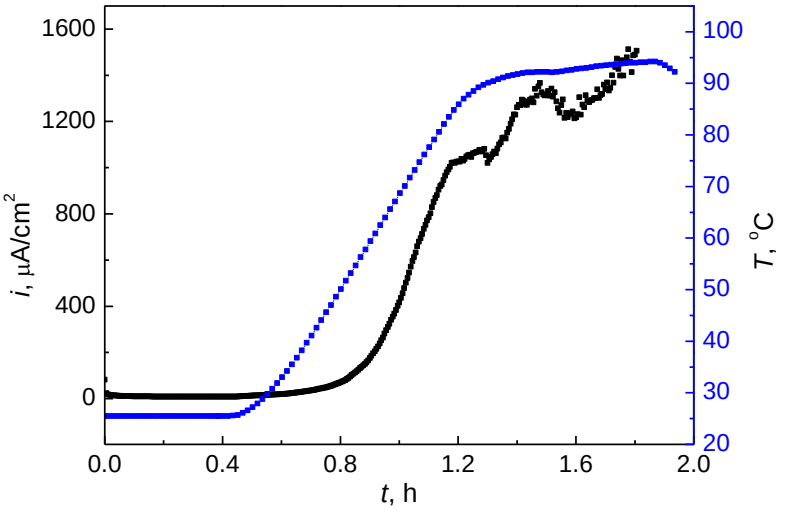

Figure 5. The *i-t* and *T-t* curves of 316 L in H_2S-containing condition at different temperatures. The partial pressures of H_2S and CO_2 are 100 kPa and 500 kPa, respectively.

3.2 Coexistence of H_2S and Cl^- on the corrosion behavior of SS

3.2.1 Electrochemical tests

Fig. 6 shows the potentiodynamic polarization curves of 316L stainless steel in solutions under different gas conditions and different Cl^- concentrations at 120°C. The parameters extracted from the anodic branch, including corrosion potentials (E_{corr}), passive current densities (i_p), pitting potentials (E_p) and repassivation potentials (E_{rp}) are listed in Table 2. The i_p values increase with Cl^- under N_2

conditions from 6.84 to 43.5 μA/cm^2, indicating the existence of Cl^- can promote the corrosion process. In the presence of H_2S, i_p increases dramatically to 575 μA/cm^2, indicating the protectiveness of passive film decreases in H_2S-containing environment. Under N_2 and 5000 mg/L Cl^- condition, the passive region is the widest, indicating that 316L is more pitting resistant. When Cl^- content increased to 130,000 mg/L, the passive region is narrowed, i.e., the pitting potential decreased from -45 mV (vs. Ag/AgCl) to -228 mV (vs. Ag/AgCl), indicating that Cl^- would promote pitting corrosion. In H_2S-containing condition, when Cl^- concentration was increased to 130,000 mg/L, the passive region is slightly narrowed. Moreover, the repassivation potential is lower than corrosion potential, indicating the worse repassivation ability of 316L in this condition. Wang [18] has found the similar behavior of 316L stainless steel in SO_2 condition. They believed the lower repassivation potential is attributed to the existence of pits after the polarization tests. Accordingly, the repassivation ability is worst in 130,000 mg/L Cl^-, H_2S saturated condition. Therefore, both H_2S and Cl^- can promote the occurrence of pitting. The corrosion resistance of the 316L was the worst under the coexistence of H_2S and Cl^-.

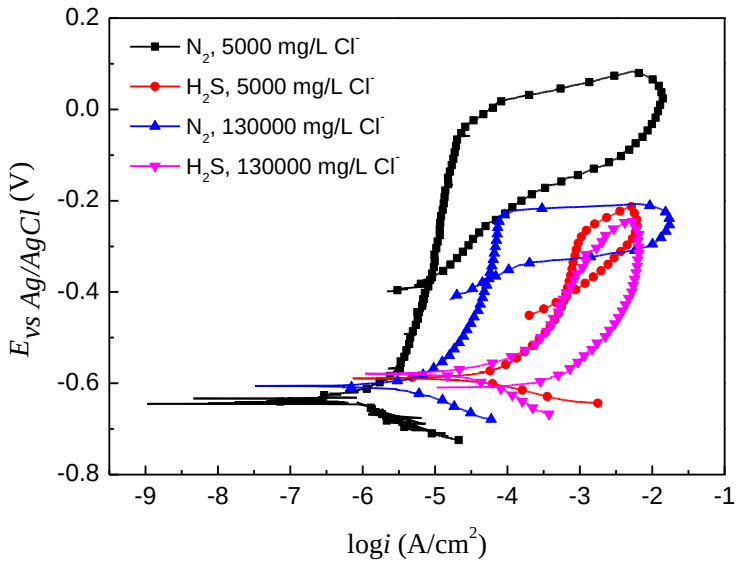

Figure 6. The polarization curves of 316L stainless steel under different conditions at 120°C. In H_2S-containing condition, the partial pressures of H_2S and CO_2 are 100 kPa and 500 kPa, respectively.

Table 2. Corrosion parameters extracted from the cyclic polarization curves

Gas	Condition Cl^- concentration, mg/L	E_{corr}, V	E_p, V	E_{rp}, V	i_p, μA/cm^2
N_2	5,000	-0.645	-0.045	-0.362	6.84
H_2S	5,000	-0.590	-0.276	-0.402	575
N_2	130,000	-0.606	-0.228	-0.368	43.5
H_2S	130,000	-0.579	-0.310	-0.606	575

Fig. 7 shows the Nyquist plots of 316L stainless steel in solutions under different gases condition and different Cl^- concentration. The EIS data were fitted by the electrochemical equivalent circuit. After comparing multiple equivalent circuit diagrams, the diagram with the minimum error was chosen. The diagram in Fig. 8 has also been proposed and used in other researches [19]. As shown in Fig. 8, R_s is the solution resistance, CPE (Q_f) is relate to the capacitance of passive film, and R_f is the resistance of passive film. CPE (Q_{d1}) is the capacitance of electrical double layer at interfaces, and R_t is the charge transfer resistance.

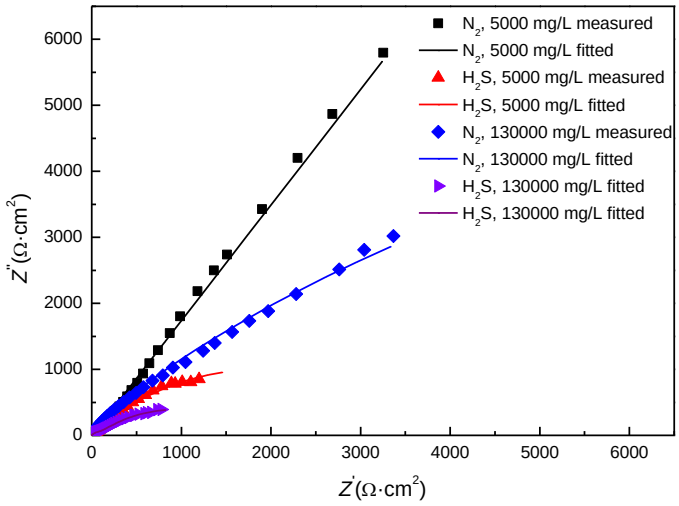

Figure 7. The Nyquist plots of 316L stainless steel in solutions under different conditions at 120°C. In H_2S-containing condition, the partial pressures of H_2S and CO_2 are 100 kPa and 500 kPa, respectively.

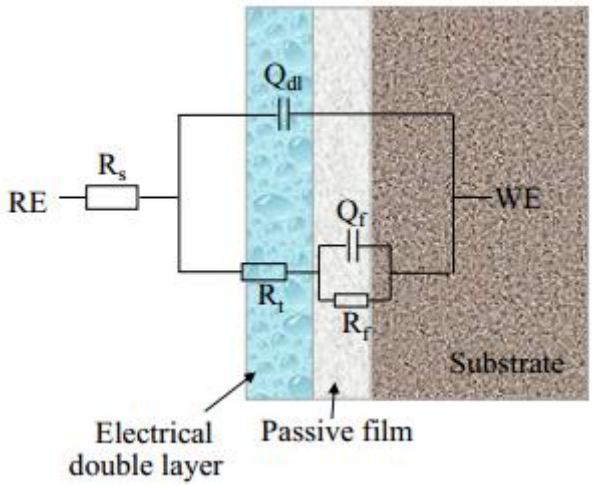

Figure 8. Equivalent circuit for simulating EIS results

CPE (Q) is commonly used in the case of uneven current distribution at the surface or in the case of increased surface roughness. The impedance of CPE is given by:

$$Z_Q = Y_0(j\omega)^{-n}$$

where Y_0 is a modulus, j^2=-1, ω is the angular frequency, n is an empirical exponent between 0 and 1. When n = 1, the CPE represents a pure capacitor. When n = 0, the CPE represents a resistor, and when n = 0.5 the CPE represents Warburg impedance. The values of the equivalent circuit elements for each data are presented in Table 3.

Table 3. Calculated equivalent circuit parameters

Condition		R_s, Ω cm^2	Q_{dl}		R_t, kΩ cm^2	Q_f		R_f, kΩ cm^2
Gas	Cl^- concentration/mg/L		Y_0 ($\Omega^{-1}cm^{-2}$ s^n)	n		Y_0 ($\Omega^{-1}cm^{-2}$ s^n)	n	
N_2	5,000	7.43	9.78×10^{-4}	0.67	4.47	5.40×10^{-4}	0.83	78.8
H_2S	5,000	6.85	7.22×10^{-4}	0.74	0.24	1.67×10^{-4}	0.60	3.64
N_2	130,000	6.83	2.46×10^{-4}	0.92	1.12	7.22×10^{-4}	0.49	26.6
H_2S	130,000	6.15	3.68×10^{-4}	0.80	0.11	3.09×10^{-4}	0.53	1.71

The diameter of the impedance arc is largest in N_2 and 5,000 mg/L Cl^- solution. R_t and R_f values were 4.47 and 78.8 kΩ, respectively. When the Cl^- concentration increased to 130,000 mg/L, the impedance arc obviously became smaller, and R_f value decreased from 78.8 to 26.6 kΩ, indicating that Cl^- concentration can decrease the corrosion resistance. When in the H_2S-containing condition, the impedance arc became much smaller. R_f decreased to 0.80 and 1.71 kΩ, indicating that the protectiveness of passive film was much degraded in H_2S-containing condition.

3.2.2 Surface morphology

Fig. 9 shows the surface morphology of 316L stainless steel immersed at 120 ^oC, 130,000mg/L Cl^- condition after 30 days. Under N_2 environment, the sample surface still had metallic luster and no pit was observed.

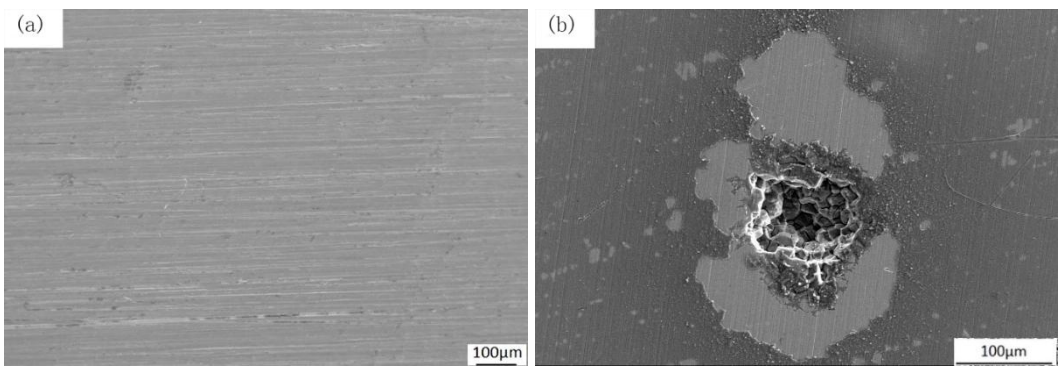

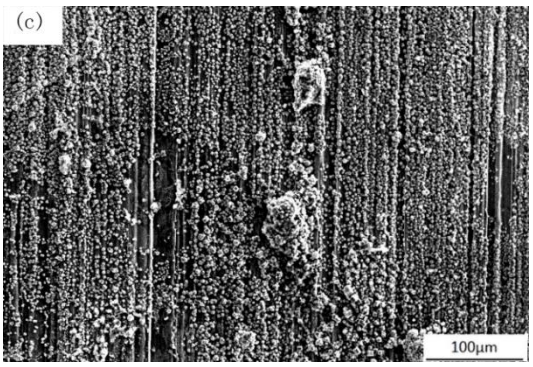

Figure 9. The surface morphology of 316L stainless steel samples immersed at 120°C, 130,000mg/L Cl^- condition after 30 days: (a) H_2S-free, (b) 30kPa H_2S and 150 kPa CO_2, (c) 100 kPa H_2S and 500 kPa CO_2.

The scratch on the surface indicated that 316L had good corrosion resistance in this condition. When the partial pressure of H_2S is 30 kPa, the surface of the samples became dim and pits were found. However, when the H_2S partial pressure was further increased to 100 kPa, no pits were observed. However, some corrosion products precipitated on the surface, demonstrating that the protectiveness of the passive film was much degraded. This result is in accordance with the electrochemical tests.

3.2.3 XPS analysis results

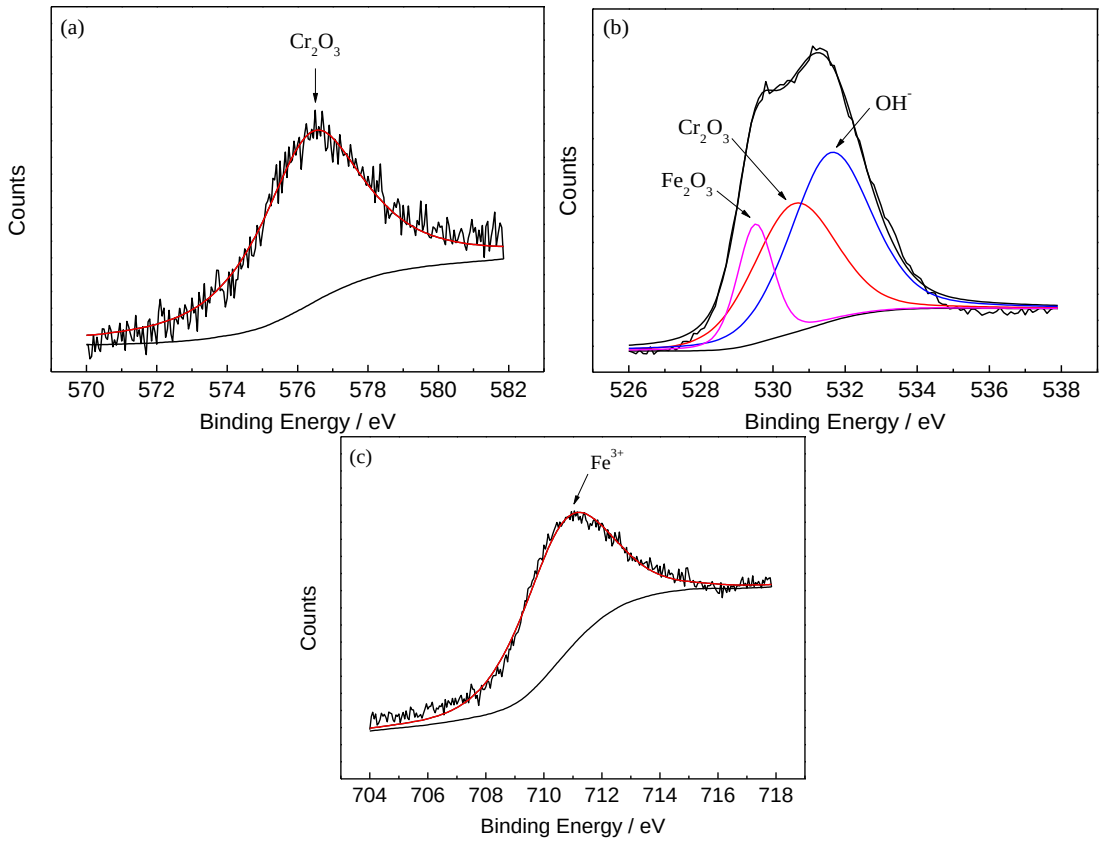

Figure 10. XPS spectra of passive films formed on 316L stainless steel under natural air condition: (a) Cr 2p, (b) O1s, and (c) Fe 2p.

XPS analysis was employed to investigate the deterioration of passive film by clarifying the chemical composition of the passive films formed under H_2S-containing conditions. XPS samples were prepared after 24 h's exposure in the air. Then XPS analysis was employed on samples to investigate the chemical composition of the passive film formed under natural air condition. The other samples were immersed in the corrosive system and then extracted 30 d later. Therefore, the comparison of the above XPS results can provide information on the passive film evolution. Fig. 10 shows the high-resolution spectra for (a) Cr 2p3/2, (b) O1s, and (c) Fe 2p3/2 recorded on the samples exposed in the air for 24 h. The Cr 2p peak at a binding energy of 576.4 eV can be attributed to Cr_2O_3 [20, 21]. The O1s spectrum shown in Fig. 7b is fitted to three peaks, namely, Fe_2O_3 (529.5 eV), Cr_2O_3 (530.7 eV) and OH^- (531.6 eV). The curve fitting in Fig. 7c shows that the peak at 710.7 eV is attributed to Fe^{3+} [[9]]. The passive film formed in natural air mainly consists of Fe_2O_3, $Fe(OH)_3$ and Cr_2O_3.

Fig. 11 shows the high-resolution spectra for (a)Fe 2p3/2, (b)Cr 2p3/2, (c)Ni 2p3/2 and (d)S 2p recorded on the samples immersed at 120°C, 100 kPa H_2S and 500 kPa CO_2, 130,000mg/L Cl^- condition after 30 days. The Fe 2p spectra is fitted to two peaks, presenting Fe^{2+} (709.5 eV) and Fe (706.7 eV). The Cr 2p peak at a blinding energy of 576.4eV can be attributed to Cr_2O_3. The Ni 2p spectra, shown in Fig. 7c, can be separated into three peaks, contributing to NiO (853.3 eV), NiS (853.1 eV) and Ni (856.5 eV).

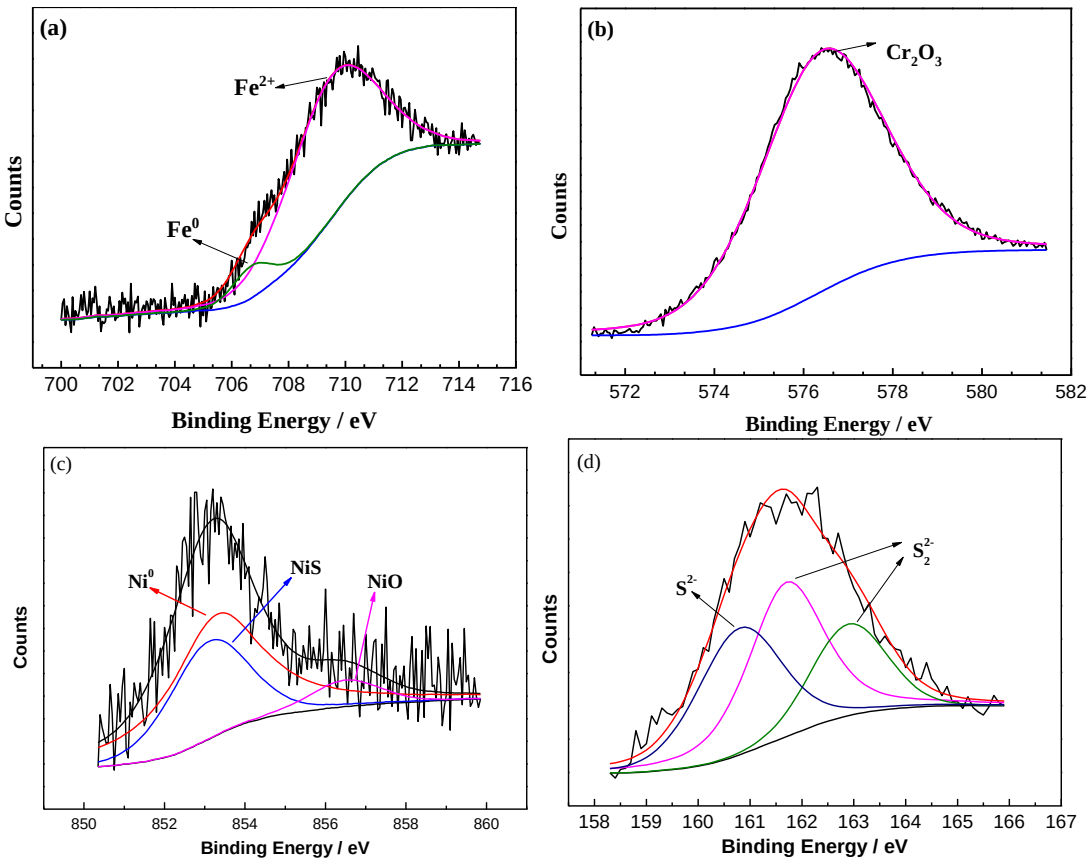

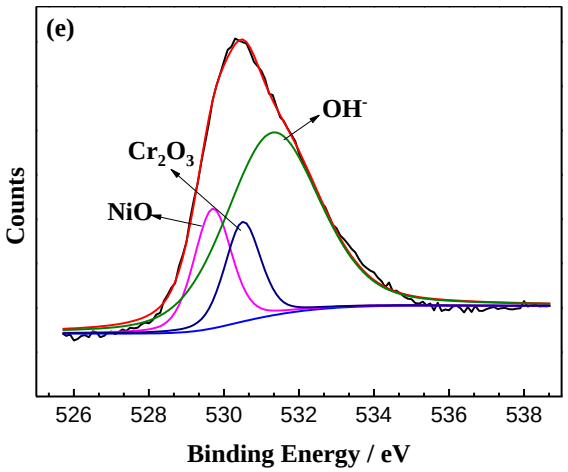

Figure 11. XPS spectra of passive film formed on 316L stainless steel samples immersed at 120°C, 100 kPa H_2S and 500 kPa CO_2, 130,000 mg/L Cl^- condition after 30 days: (a) Fe 2p3/2, (b)Cr 2p3/2, (c)Ni 2p3/2,(d)S 2p, (e)O 1s

The S 2p spectra consists of two peaks contributing to S_2^{2-} (161.7 eV) and S^{2-} (160.8). The O 1s spectra is fitted to three peaks, presenting Cr_2O_3 (530.5 eV), OH^- (531.3 eV) and NiO (529.7 eV). From the above analysis, the passive film formed at this condition was composed of FeS_2, NiO, NiS, FeS, Cr_2O_3 and $Fe(OH)_2$. This result is similar with Liang' work, who found the surface film was composed of Cr_2O_3, MoO_3, FeS, FeS_2, $Fe(OH)_2$ and FeO after immersing the sample in the sulphate-reducing bacteria medium [20]. Cr exits in the passive film in the form of Cr_2O_3 before and after the immersion test due to the stable property of Cr_2O_3. However, NiS and FeS present in the film, which indicates the passive film is sulfureted during the test.

3.2.4 AES analysis

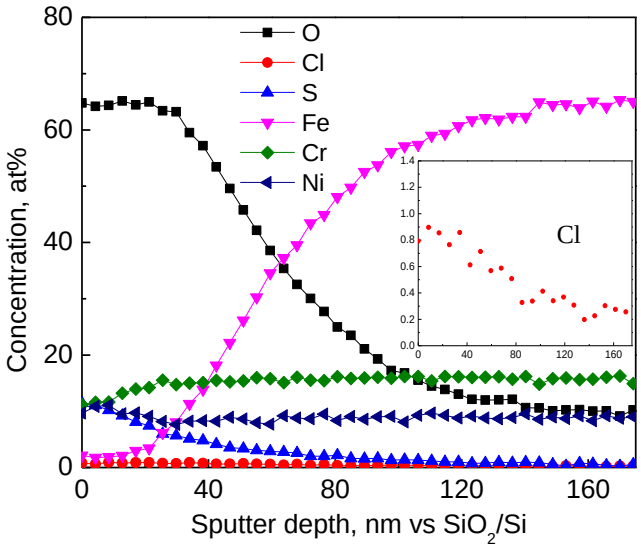

Figure 12. Auger depth profiles for passive film formed on 316L stainless steel samples immersed at 120°C, 100 kPa H_2S and 500 kPa CO_2, 130,000mg/L Cl^- condition after 30 days.

AES surface depth profiles were examined to identify the distribution of alloyed elements in the passive film of 316L stainless steel. Fig. 12 shows depth profiles of the element in the passive film of 316L stainless steel immersed at 120°C, 100 kPa H_2S, 130,000 mg/L Cl^- condition after 30 days. As is seen, the at% of O, S, Ni and Cl contents decrease with sputter depth, while Fe and Cr do conversely. The Fe at% in the outermost layer is very low, which is due to the consumption and dissolution of Fe. The Ni at% is slightly higher in the film than the metal matrix, which may be attributed to the precipitate of NiS on the surface. The oxide film thickness was determined to be approximately the depth at which the oxygen concentration reaches 50% of its maximum value [22]. Accordingly, the thickness of the passive film is about 68 nm. It is generally believed that Cl^- has an affinity to metals [23], so it can accelerate active dissolution and promote passive film to be thinner and less protective [24, 25]. According to the PDM model [26], H_2O can promote the passivation of 316L stainless steel. However, under H_2S containing condition, H_2S can compete with H_2O to combine with metal ions so that the formation of oxide was inhibited to some extent. The adsorption of anions depends on the corresponding polarizability. Polarizability of sulfides is reported to be higher than that of OH^- [27]. Therefore, the 316L stainless steel has higher pitting corrosion risk because of a synergistic effect of H_2S and Cl^-.

4. CONCLUSIONS

The corrosion behavior of 316L stainless steel under the condition of coexistence of H_2S and Cl^- has been studied in NaCl solution with H_2S by different electrochemical measurements, XPS and AES for surface analysis. The major results are concluded as follows.

(1) 316L is temperature sensitive at around 110°C in H_2S-free condition. The presence of H_2S can make 316L much more sensitive to temperature.

(2) Both H_2S and Cl^- can decrease the corrosion resistance of 316L. The synergistic effect has been found in the coexistence of H_2S and Cl^-.

(3) The XPS results revealed that the passive film formed on the 316L samples immersed in 120°C, 100 kPa H_2S, 130,000 mg/L Cl^- condition was composed of FeS_2, NiO, NiS, Cr_2O_3 and $Fe(OH)_2$.

(4) The AES results revealed that elemental S and Cl can penetrate into the passive film. Cl^- can accelerate active dissolution and promote passive film to be thinner and H_2S can compete with H_2O to combine with metal ions so that the formation of oxide was inhibited, which presents a synergistic effect of H_2S and Cl^-.

ACKNOWLEDGEMENT
This work was supported by National Natural Science Foundation of China (Grant No. 51271025) and National Science and Technology Major Project (No. 2016ZX05028-004-005).

References

1. Q. Wang, X. Wang, H. Luo and J. Luo, *Surf. Coat. Tech.*, 291 (2016) 250.

2. X. Hu and A. Neville, *Wear*, 267 (2009) 2027.
3. A. Kopliku, M. Tabinor, J. Ryder and P. Dent, High strength modified martensitic stainless steel production tubing for sour wells, CORROSION 2009, Atlanta, America, 2009, 14.
4. Z. Y. Liu, C. F. Dong, X. G. Li, Q. Zhi and Y. F. Cheng, *J. Mater. Sci.*, 44 (2009) 4228.
5. H. B. Gunay, P. Ghods, O. B. Isgor, G. J. C. Carpenter and X. Wu, *Appl. Surf. Sci.*, 274 (2013) 195.
6. X. Feng, Y. Zuo, Y. Tang, X. Zhao and X. Lu, *Electrochim. Acta*, 58 (2011)258.
7. M. Liu, X. Cheng, X. Li, Y. Pan and J. Li, *Appl. Surf. Sci.*, 389 (2016)1182.
8. G. T. Burstein, I. M. Hutchings and K. Sasaki, *Nature*, 407 (2000)885.
9. H. Luo, C. Dong, K. Xiao and X. Li, *RSC Adv.*, 6 (2016)9940.
10. Y. Behnamian, A. Mostafaei, A. Kohandehghan, B. S. Amirkhiz, J. Li, R. Zahiri, E. Aghaie, W. Zheng, D. Guzonas, M. Chmielus, W. Chen and J. L. Luo, *J. Supercrit Fluid*, 120 (2017) 161.
11. Y. Ashida, L. G. McMillion and M. L. Taylor, *Electrochem. Commun.*, 9 (2007) 1102.
12. X. Zhang and D. W. Shoesmith, *Corros. Sci.*, 76 (2013)424.
13. C. O. A. Olsson and D. Landolt, *Electrochim. Acta*, 48 (2003) 1093.
14. J. Hesselbach, H. W. Hoffmeister and M. Hlavac, *Prod. Eng.*, 12 (2005) 1.
15. J. Banaś, U. Lelek-Borkowska, B. Mazurkiewicz and W. Solarski, *Electrochim. Acta*, 52 (2007) 5704.
16. W. He, O. Ø. Knudsen and S. Diplas, *Corros. Sci.*, 51 (2009) 2811.
17. J. Ding, L. Zhang, M. Lu, J. Wang, Z. Wen and W. Hao, *Appl. Surf. Sci.*, 289 (2014)33.
18. Z. Wang, X. Tang, J. Xue, L. Zhang, T. Li and M. Lu, The pitting behavior of stainless steels under SO_2 environments with Cl^- and F^-, CORROSION 2017, Vancouver, Canada, 2017, 10.
19. M. Sanchez, J. Gregori, C. Alonso, J. J. Garcia-Jareno, H. Takenouti and F. Vicente, *Electrochim. Acta*, 52 (2007) 7634.
20. L. Cheng-hao, W. Hua and H. Nai-bao, *J. Iron Steel Res. Int.*, 21 (2014) 444.
21. M. Ben Salah, R. Sabot, P. Refait, I. Liascukiene, C. Methivier, J. Landoulsi, L. Dhouibi and M. Jeannin, *J. Electrochem. Soc.*, 99 (2015) 320.
22. S. Mischler, A. Vogel, H. J. Mathieu and D. Landolt, *Corros. Sci.*, 32 (1991) 925.
23. H. H. Uhlig, *J. Electrochem. Soc.*, 97 (1950) 215C.
24. G. S. Frankel, *J. Electrochem. Soc.*, 145 (1998)2186.
25. J. Soltis, *Corros. Sci.*, 90 (2015) 5.
26. D. D. Macdonald, S. R. Biaggio and H. Song, *J. Electrochem. Soc.*, 139 (1992) 170.
27. J. Lee, Y. Kitagawa, T. Nakanishi, Y. Hasegawa and K. Fushimi, *J. Electrochem. Soc.*, 162 (2015) C685.